A Synoptic Climatology of the Subtropical Kona Storm

JASON A. OTKIN AND JONATHAN E. MARTIN

Department of Atmospheric and Oceanic Sciences, University of Wisconsin—Madison, Madison, Wisconsin

(Manuscript received 23 April 2003, in final form 12 January 2004)

ABSTRACT

Ten years of surface and upper-air analyses from the ECMWF Tropical Ocean Global Atmosphere (TOGA) dataset were used to construct a synoptic climatology of kona storms in the subtropical central and eastern Pacific Ocean. Within a sample of 115 cyclones that predominantly occurred during the Northern Hemisphere cool season, three distinct types of kona storms were identified: cold-frontal cyclogenesis (CFC) cyclones, cold-frontal cyclogenesis/trade wind easterlies (CT) cyclones, and trade wind easterlies (TWE) cyclones. Of the three types, CFC cyclones were found to be the most common type of kona storm, while CT and TWE cyclones occur much less frequently.

The geographical distribution, propagation characteristics, and the monthly and interannual variability in the number of kona storms are presented. Kona storms initially develop across a large portion of the subtropical Pacific, with the greatest concentration of kona storms found within a southwest-to-northeast-oriented band from west of Hawaii to 40°N, 140°W. A distinct latitudinal stratification was evident for each type of kona storm, with CFC, CT, and TWE cyclones each more likely to initially develop at successively lower latitudes. The analysis reveals that kona storms can propagate in any direction but exhibit a clear preference to propagate toward the northeast. Use of the multivariate ENSO index indicates that the number of kona storms that develop during each cool season is not correlated to the phase of ENSO.

An analysis of the composite structure and evolution of each type of kona storm revealed some common and some unique characteristics. Development of the surface cyclone in all types results from the intrusion of an upper-level disturbance of extratropical origin into the subtropics, although differences in the initial structure and subsequent evolution of the 300-hPa trough were noted for each type of kona storm. The analysis also revealed that relatively weak 300-hPa winds are present throughout the evolution of each type of kona storm and that the composite kona storm tends to be nestled along the southern boundary of a region of higher surface pressure during the mature stage of its evolution. The development of robust ridges in the 300-hPa geopotential and 1000–500-hPa thickness fields downstream of the composite surface cyclone were noteworthy features that characterized the evolution of all kona storms, the latter feature strongly suggesting that these disturbances are fundamentally baroclinic in nature.

1. Introduction

During the Northern Hemisphere cool season (October–March), upper-tropospheric disturbances of extratropical origin occasionally propagate sufficiently equatorward in the Pacific Ocean basin to spawn significant, lower-tropospheric, cyclonic disturbances at subtropical latitudes. In the Hawaiian Islands, the resulting subtropical cyclones are referred to as kona[1] storms (Simpson 1952). Because of the important influence that such storms have on the climate of the Hawaiian Islands, significant attention has been directed toward examining the structure and evolution of kona storms on the mesoscale and synoptic scale with an eye toward describing the wide range of sensible weather hazards that can accompany their passage across the Hawaiian Islands. Historically, these hazards have included damaging winds, waterspouts, large surf, landslides, hailstorms, flash floods, severe thunderstorms, and even blizzards (Dangerfield 1921; Leopold 1948; Simpson 1952; Ramage 1962; Schroeder 1977a,b; Kodama and Barnes 1997; Businger et al. 1998; Wang et al. 1998; Morrison and Businger 2001).

During the evolution of a kona storm, the heaviest rainfall generally occurs within the moist tropical air in the southeast quadrant of the surface cyclone, with thunderstorms and squall lines possible within a region of strong convergence on the eastern side of the kona storm (Simpson 1952; Wang et al. 1998; Businger et al. 1998).

[1] "Kona" is a Polynesian adjective meaning leeward and is used to describe the condition in which the usually persistent trade wind easterlies are replaced by southerly winds and rain squalls so that locations ordinarily in the trade wind lee of mountain ranges are exposed to onshore winds. The terms "kona storm" and "subtropical cyclone" are used interchangeably during the course of this study.

Corresponding author address: Dr. Jonathan E. Martin, Dept. of Atmospheric and Oceanic Sciences, University of Wisconsin—Madison, 1225 W. Dayton Street, Madison, WI 53706.
E-mail: jon@aos.wisc.edu

© 2004 American Meteorological Society

As a consequence of the abundant moisture and deep convection, individual kona storms are capable of producing copious amounts of rainfall. For example, heavy rainfall associated with kona storms during January and February 1979 resulted in numerous rainfall records on the island of Hawaii, including a daily record of 566.4 mm at Hilo (Cram and Tatum 1979). In addition, Kodama and Barnes (1997) have shown that kona storms are the dominant synoptic factor associated with heavy rain events on the southeast slopes of the Mauna Loa volcano on the island of Hawaii.

Kona storms also have a significant impact on the seasonal and annual precipitation of the Hawaiian Islands. For instance, in a detailed analysis of low-elevation rainfall on the island of Oahu, Riehl (1949) showed that over two-thirds of the annual rainfall total on the leeward side of the island results from only a few large rainstorms each winter primarily associated with kona storms. Lyons (1982) also found that southwest wind disturbances (kona storms and cold fronts) produce abundant rainfall throughout most of Hawaii during winters that are characterized by above-normal precipitation. Likewise, Chu et al. (1993) found that numerous (zero) ''kona days'' occurred during two winter seasons (defined as January–February) characterized by above (below) normal precipitation at Honolulu and Lihue.

Simpson (1952) recognized that kona storms are a major feature of the subtropical circulation and provided the first synoptic climatology of the structure and evolution of these cyclones. In that pioneering study, standard surface observations and a limited number of upper-air soundings were used to survey 76 kona storms that occurred over a 20-yr period near the Hawaiian Islands. From this survey, two distinct types of kona storms were distinguished from each other by differences in the initial development of the surface cyclone. With the most common type (48 cyclones), cyclogenesis occurs when an occluded surface cyclone becomes trapped in the low latitudes by the blocking action of a warm ridge to its north. Less often (28 cases), cyclogenesis occurs either in the trade wind easterlies because of the downward extension of the circulation associated with a strengthening upper-level cyclone or at the southern extremity of a polar trough that has extended far equatorward. Regardless of which type of cyclogenesis occurs, the evolution of the kona storm is usually characterized by the seclusion of the mature cyclone from sources of cold air to its north. The end of the kona life cycle is often characterized by the merger of the kona cyclone with a transient midlatitude trough or less often by the slow decay of the mature cyclone. Simpson's analysis also showed that kona storms generally possess a cold-core structure with the strongest circulation in the middle and upper troposphere.

Despite the fact that kona storms have a significant impact on Hawaiian climate and play an important role in the subtropical circulation, more than half a century has passed without any update to Simpson's original climatology. In order to provide fresh insight into the structure and evolution of kona storms, and to examine the large-scale environment within which they evolve, this paper presents the results of a 10-yr census of kona storms in the subtropical central and eastern Pacific (SCEP) Ocean. The paper is organized as follows: In section 2, we describe the dataset and analysis method used to construct the synoptic climatology presented in this paper. Aspects of the intraseasonal and interannual frequency, geographical distribution, and propagation characteristics of kona storms are presented in section 3. An analysis of the composite structure and evolution of kona storms is presented in section 4. Section 5 contains a companion analysis of the composite evolution from a potential vorticity (PV) perspective. Finally, a discussion and conclusions are presented in section 6.

2. Data and methodology

Surface and upper-air analyses from the European Centre for Medium-Range Weather Forecasts (ECMWF) Tropical Ocean Global Atmosphere (TOGA) dataset for 10 yr from 1986 to 1996 were used to construct the climatology presented here. The ECMWF dataset consists of twice-daily (0000 and 1200 UTC) sea level and 14–15 unequally spaced pressure-level analyses with global 2.5° latitude–longitude resolution that are directly interpolated from the ECMWF operational, full-resolution surface and pressure level data.[2] As such, these fields are subject to changes in the ECMWF data assimilation scheme. The TOGA data incorporates data from a wide range of sources including standard synoptic reports, radiosonde data, and ship and aircraft reports. Of particular importance for the present study is the inclusion of satellite data from the Television Infrared Operation Satellite (TIROS) Operational Vertical Sounder (TOVS) and the Special Sensor Microwave Imager (SSM/I). Radiances from these remote sensing platforms were collected throughout the period investigated here and provide crucial observations over the data-sparse Pacific. These data constitute a substantial improvement over that which was available to Simpson 50 years ago and thus provide a solid basis for an update to his climatology of kona cyclones.

For this study, a cyclone was defined to be a minimum in the sea level pressure (SLP) field surrounded by at least one closed isobar (analyzed at 2-hPa intervals). To qualify as a kona storm, the surface cyclone had to initially develop within a portion of the SCEP (10°–40°N, 160°E–130°W, hereafter referred to as the SCEP domain) and then maintain a closed SLP isobar for a minimum of 48 h. In order to emphasize the subtropical characteristics of kona storms, cyclones that initially developed within the northern portion of the SCEP do-

[2] The operational resolution of the ECMWF model was T63 from 1986 through 1991, when it increased to T213.

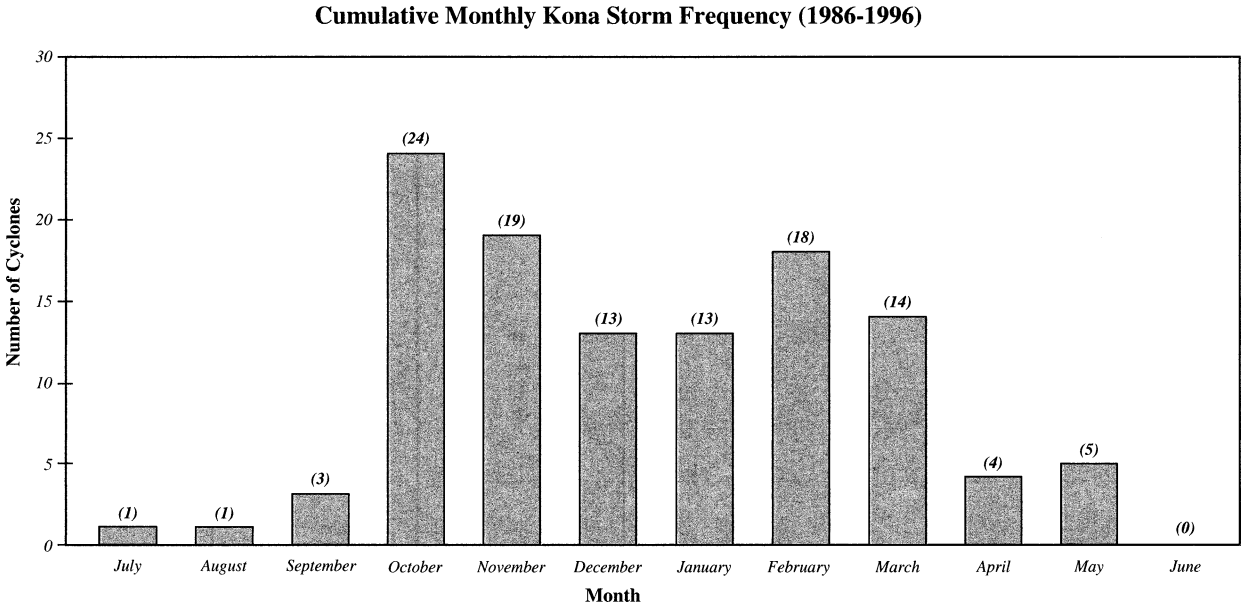

FIG. 1. Cumulative monthly kona storm frequency from the climatology.

main (between 30° and 40°N) were also required to attain their lowest SLP south of 40°N. Those cyclones that initially developed south of 30°N, however, were not subject to this additional constraint. All surface cyclones that initially developed outside of the subtropical Pacific before propagating into the SCEP domain were excluded from the climatology. Finally, all tropical cyclones were removed by comparing cyclone locations to the Hurricane Best Track Files for the eastern Pacific obtained from the National Weather Service's Tropical Prediction Center.

The population of cyclones that satisfied each of these requirements was then subjectively separated into three categories that are distinguished from each other by differences in the initial development of the surface cyclone. If the surface cyclone initially developed along a cold front extending southward from a midlatitude cyclone and then propagated primarily in an *eastward* direction, the cyclone was designated as a cold-frontal cyclogenesis (CFC) case. However, if a cyclone was characterized by initial development along a cold front followed by primarily *westward* propagation during the early stages of its life cycle, the cyclone was classified as a cold-frontal cyclogenesis/trade wind easterly (CT) case. Finally, if the initial cyclogenesis occurred completely within the trade wind easterlies, with no evidence for development along a preexisting cold front, the cyclone was designated as a trade wind easterly (TWE) case. Based upon the foregoing definitions, 87 CFC, 23 CT, and 5 TWE cyclones, for a total of 115 kona storms, were identified within the SCEP during the 10 yr.

TABLE 1. The number of kona storms that developed during each individual month and year in the climatology.

Season	Oct	Nov	Dec	Jan	Feb	Mar	Total
1986/87	0	2	1	0	2	2	7
1987/88	3	0	2	2	1	0	8
1988/89	2	1	0	0	4	0	7
1989/90	2	2	1	2	3	1	11
1990/91	3	4	2	2	0	1	12
1991/92	4	0	3	0	1	1	9
1992/93	2	3	3	3	0	3	14
1993/94	3	5	0	1	0	1	10
1994/95	4	1	0	0	4	3	12
1995/96	1	1	1	3	3	2	11

3. Results

a. Frequency

The cumulative monthly distribution of all kona storms that developed within the SCEP during the 10-yr climatology is shown in Fig. 1. This distribution clearly illustrates a preference for kona storms to occur during late autumn (October–November) with a secondary maximum in cyclone frequency during February. It is also noteworthy that relatively few kona storms develop during the middle of winter (December–January). Such a midwinter minimum in kona storms appears to differ markedly from the climatology presented by Simpson (1952), who actually notes a January maximum in kona storms (see his Table 1). It is important to note, however, that Simpson's analysis occurred over a smaller domain centered on the Hawaiian Islands. Given the available data at the time, his analysis likely underrepresented the number of events that occur north of Hawaii during fall and spring. The more comprehensive dataset available for this study, combined with its larger domain, are thought to be important contributors to these differences. In Table 1, the number of

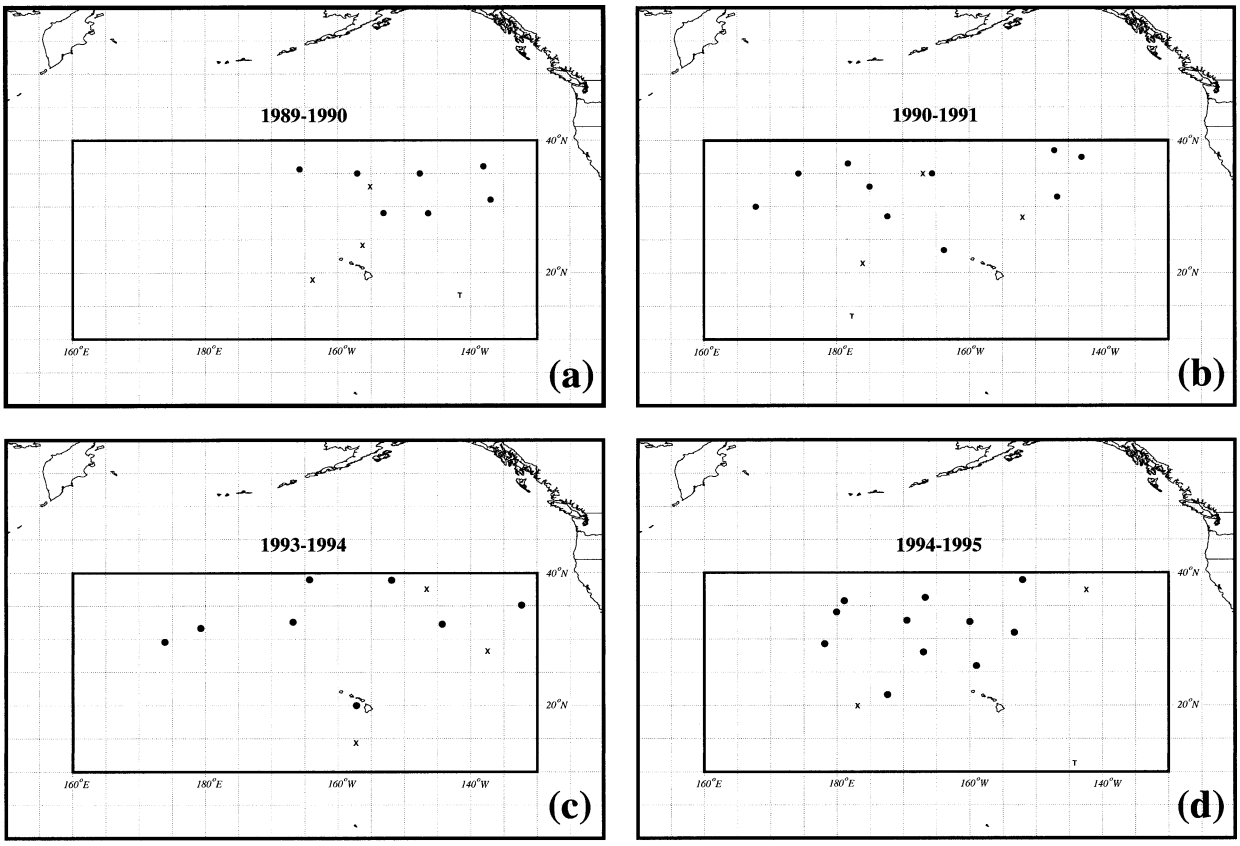

FIG. 2. Yearly distributions of kona cyclones in (a) 1989/90, (b) 1990/91, (c) 1993/94, and (d) 1994/95. Filled circles represent CFC cyclones, bold X's represent CT cyclones, and bold T's represent TWE cyclones. Boxed area is the SCEP domain described in the text.

kona storms that developed during each individual month and cool season within the 10-yr climatology is given. Inspection of the monthly data reveals substantial intraseasonal variability in kona cyclone frequency. This variability is demonstrated by the dramatic month-to-month fluctuations in kona cyclone frequency that occur during many of the cool seasons (such as 1991/92). It is also noteworthy that 18 individual months within the 10 cool seasons were characterized by the development of three or more Kona storms, whereas no Kona storms developed during 15 other cool-season months. Year-to-year fluctuations in the number of Kona storms that develop each cool season also indicate that considerable interannual variability in Kona cyclone frequency occurs.

b. Geographical distribution

In this section, the geographical distribution of all kona storms at the initial cyclogenesis, mature, and final cyclolysis stages of cyclone evolution is presented. For each cyclone, ''initial cyclogenesis location'' was defined to be the location where the first closed sea level isobar was identified, the ''mature location'' was identified as the location of the SLP minimum,[3] and the ''final cyclolysis location'' refers to the location at which the last closed sea level isobar was identified. In order to document the geographical distribution of each type of kona storm, CFC cases are represented as closed circles, CT cases as X's, and TWE cases as T's in all subsequent figures.

The interannual geographical variability of initial kona cyclogenesis is considerable. Rather than display the distribution for all 10 seasons, only two representative examples are illustrated. In the first example, Kona storms exhibit substantial longitudinal variability between 1989/90 (Fig. 2a, when all cyclones were confined to the eastern portion of the SCEP domain) and 1990/91 (Fig. 2b, when most kona storms were located west of 160°W). Another example of the geographic variability is the seemingly random distribution of kona

[3] For a small subset of cyclones that propagated along a strong SLP gradient, it was found that the occurrence of the SLP minimum was not always representative of the mature stage of the cyclone's evolution. Therefore, for these cyclones, the occurrence of the strongest circulation at sea level was subjectively determined and then used in place of the SLP minimum as representing the mature stage of the cyclone.

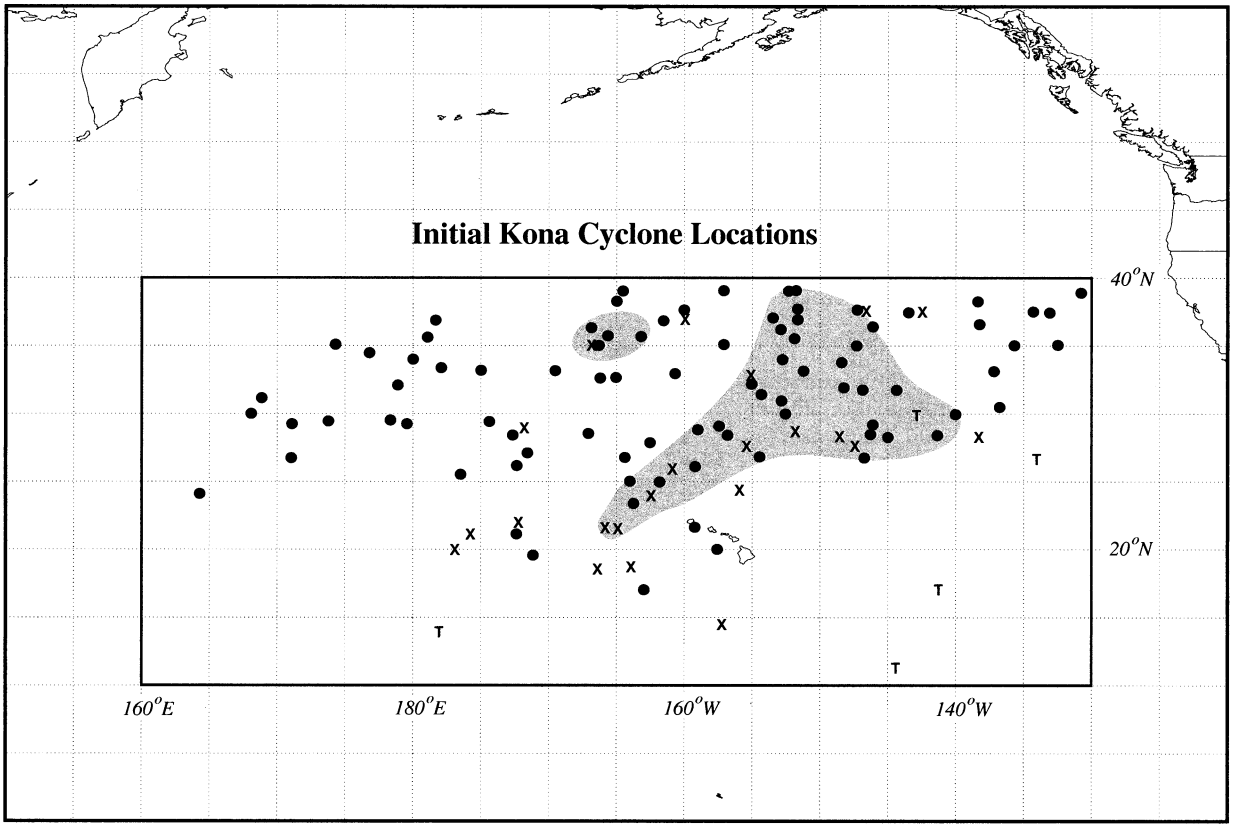

FIG. 3. Initial kona cyclone locations from the climatology. Bold circles represent locations of CFC cyclones, bold X's represent locations of CT cyclones, and bold T's represent locations of TWE cyclones. Shading indicates the region with the greatest concentration of kona cyclogensis locations.

storms across the SCEP domain during 1993/94 (Fig. 2c) compared to the more compact distribution of kona storms in the center of the SCEP domain during 1994/95 (Fig. 2d).

The cumulative distribution of initial cyclone locations for the entire 10-yr climatology is shown in Fig. 3. This distribution clearly illustrates that kona storms frequently develop across a large portion of the subtropical Pacific, with the greatest concentration of kona storms occurring within a southwest-to-northeast-oriented band (indicated by shading in Fig. 3) from west of Hawaii to approximately 40°N, 140°W. Close inspection of this analysis reveals a distinct stratification of each type of kona storm into certain latitude bands. For example, CFC cyclones generally experience their initial cyclogenesis north of 25°N, CT cyclones typically originate between 15° and 30°N, while TWE cyclogenesis is confined to the region south of 20°N or within the southeast portion of the SCEP domain.

The mature location of each kona storm is shown in Fig. 4. At this stage of their life cycle, most kona storms are concentrated along the northern portion of the SCEP domain with only a few CT and TWE cyclones still located south of 25°N. It is interesting to note that even though kona storms are a critical component of the Hawaiian climate, no kona storms reached the mature stage of development directly over the Hawaiian Islands during the 10-yr climatology. By the final cyclolysis stage (Fig. 5), kona storms are uniformly distributed across the eastern half of the Pacific basin, which indicates that cyclolysis does not occur within a favored geographical region for the population as a whole. However, it is noteworthy that a large number of CT cyclones experienced their final cyclolysis within a small region west of Hawaii.

c. Propagation characteristics

To illustrate the propagation characteristics of kona storms, Simpson (1952) presented the tracks of several representative cyclones from within his population of kona storms. This method, however, is much too cumbersome to provide a comprehensive survey of the numerous kona storms in the present study. Therefore, in order to provide a compact analysis of kona storm propagation characteristics, a new graphical representation that we have termed the ''propagation rose'' has been constructed.

The construction of a propagation rose is a two-step process. First, the distance and direction that each cy-

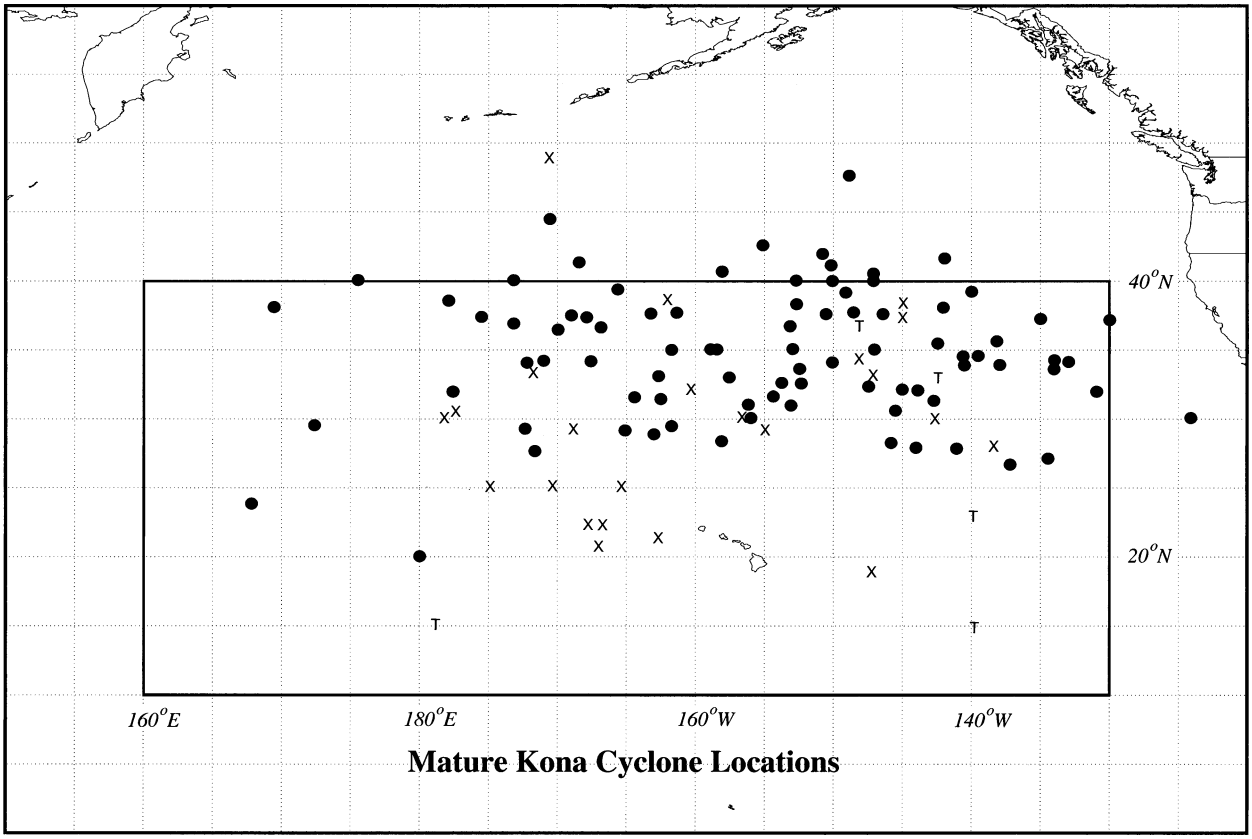

FIG. 4. Mature kona cyclone locations from the climatology. Filled circles represent locations of CFC cyclones, bold X's represent locations of CT cyclones, and bold T's represent locations of TWE cyclones.

clone propagates from one time to another is calculated. After this is completed for the entire population of cyclones, the results are then separated into a finite number of distance and direction categories. In the present study, for example, the propagation rose was constructed using four distance categories within 12 individual direction categories (each consisting of 30° slices). Although the method used to construct the propagation rose undoubtedly smooths out any small-scale ''wiggles'' in the cyclone track, this representation provides a compact and useful measure of the cyclone propagation characteristics. For instance, the number of cyclones that propagated within a given distance and direction category can easily be determined. From this, the existence of any favored propagation distances and/or directions for the entire population of cyclones can also be determined.

The propagation rose shown in Fig. 6 was constructed by calculating the distance and direction that each of the 115 kona storms propagated from their initial cyclogenesis to final cyclolysis locations. Although this depiction of cyclone propagation clearly indicates that kona storms can propagate in any direction, there is a definite preference for kona storms to propagate in a northeastward direction. In fact, the four direction categories encompassing the northeast quadrant of the propagation rose account for 71 of the kona storms. It is also evident that most kona storms (102 cases) propagate less than 3000 km during their entire evolution, with a smaller subset (30 cases) propagating less than 1000 km. Several cyclones (13 cases), however, did propagate more than 3000 km, most often in a northeastward direction. In addition, the two cyclones that propagated over 3000 km in a northwestward direction illustrate that kona storms are capable of propagating westward for long distances.

d. ENSO and the interannual variability of kona storms

As previously shown, analysis of the annual frequency and distribution of kona storms reveals the existence of considerable interannual variability in both the total number of events and their spatial distribution. It is not unreasonable to suggest that this low-frequency variability might be related to interannual changes in the large-scale circulation associated with the El Niño–Southern Oscillation (ENSO) phenomenon. Probable cause for such a suspicion arises from prior studies (e.g., Horel and Wallace 1981; Geisler et al. 1985; Lau and Philips 1986; Hoerling et al. 1997; Wang and Fu 2000; Kidson et al. 2002) that have shown that ENSO winters are often characterized by significant extratropical

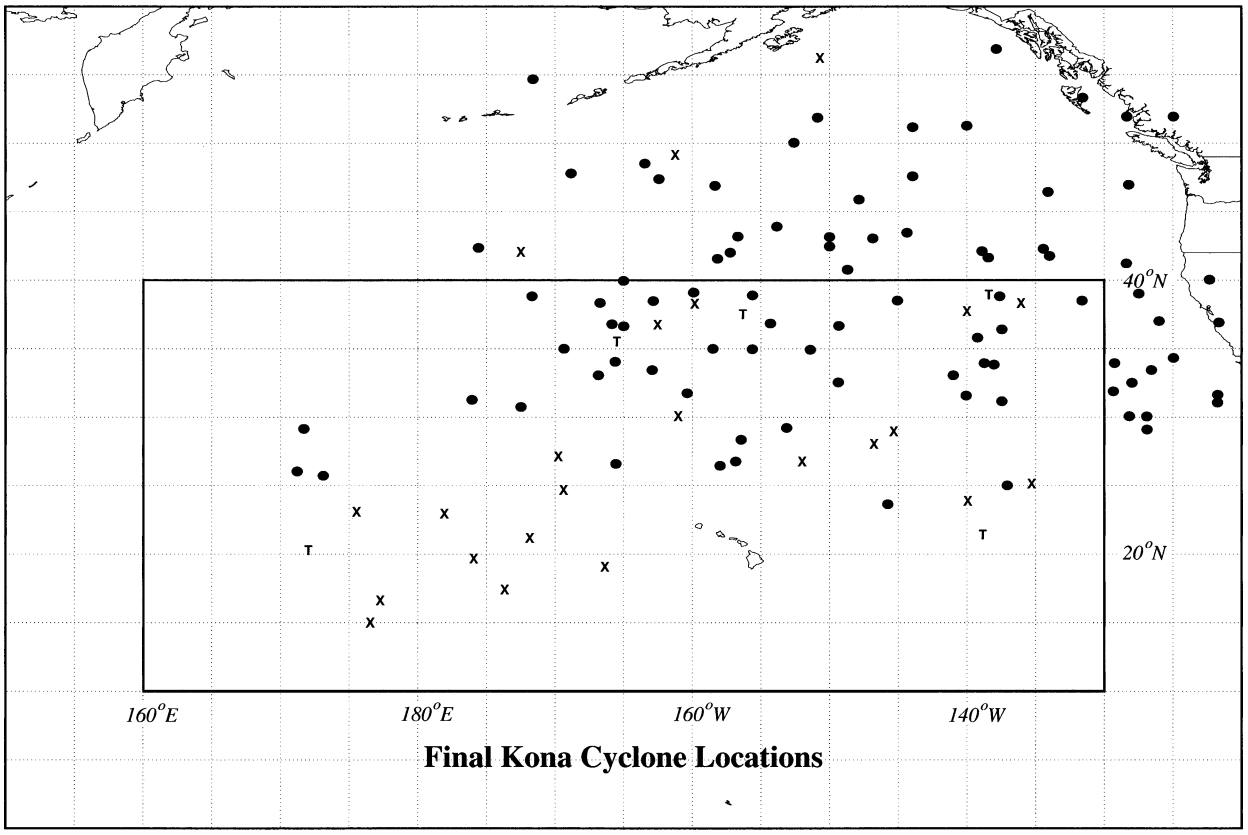

FIG. 5. Final kona cyclone locations from the climatology. Filled circles represent locations of CFC cyclones, bold X's represent locations of CT cyclones, and bold T's represent locations of TWE cyclones.

height and wind anomaly patterns across the Pacific basin. For instance, El Niño events tend to be characterized by the development of an anomalous subtropical ridge in the central Pacific, a zonally elongated Asian jet, and a strengthened Aleutian low. La Niña events, however, are often characterized by an anomalous subtropical trough in the central Pacific, a zonally retracted Asian jet, and a weakened Aleutian low. This reversal of the height and wind anomalies suggests that changes in the extratropical circulation associated with opposite phases of ENSO may modulate the occurrence of subtropical cyclones, with La Niña (El Niño) events perhaps characterized by the frequent (infrequent) occurrence of kona storms.

To explore the possible connection between ENSO and the annual frequency of kona storms, the multivariate ENSO index (MEI) was employed. The MEI is a diagnostic tool used to monitor the magnitude and phase of ENSO and is based on six primary atmospheric and oceanic variables over the tropical Pacific Ocean: sea level pressure, zonal and meridional components of the surface wind, sea surface temperature, surface air temperature, and fractional cloud cover. These six components are combined to compute the MEI for each of 12 sliding bimonthly periods (December–January, January–February, . . . , November–December) (Wolter and Timlin 1993). A positive MEI corresponds to El Niño conditions, while a negative MEI corresponds to La Niña conditions.

Figure 7 presents time series for both the average MEI and the total number of kona storms for each cool season in the climatology. Comparison of the two time series reveals a rather uncorrelated appearance, in which cool seasons associated with a certain phase of ENSO, such as La Niña, can be characterized by either an above-average (such as 1994/95) or below-average (such as 1988/89) number of kona storms. This variability, along with the extremely low linear correlation (0.016) between the two time series indicates that a relationship between ENSO and the interannual variability in the number of kona storms does not appear to exist.

4. Composite structure of kona storms

As shown previously, 87 CFC, 23 CT, and 5 TWE kona storms occurred during the 10-yr climatology. Although perusal of each set of kona storms revealed considerable intercase variability in large-scale structure and evolution (especially for CFC cyclones), some common features were also evident. In an effort to isolate these common elements, we present an analysis of the composite structure for each type of kona storm at the

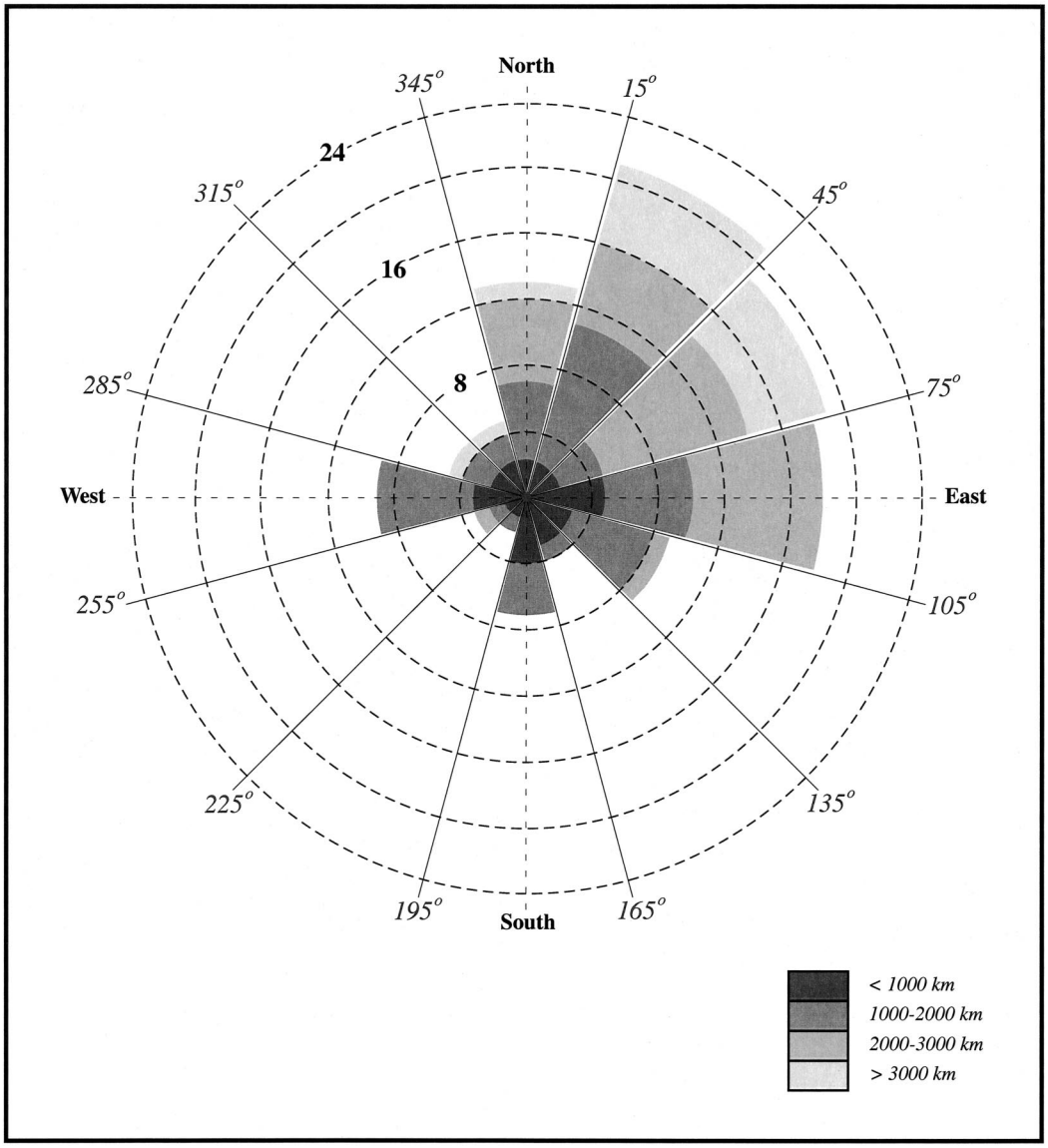

FIG. 6. Propagation rose for the population of kona cyclones in the climatology. Propagation distances are given by shading. Concentric dashed circles represent the number of cyclones in each distance and direction category.

initial development (T_{INIT}), mature ($T = 0$), and final cyclolysis (T_{FINL}) stages of cyclone evolution. Although differences in the temporal evolution of each cyclone do not allow this analysis to sequentially describe the evolution of the composite cyclone at discrete intervals (such as 12-h intervals), the structure of the composite cyclone and the large-scale environment within which it initially develops reaches the mature stage, and finally decays can still be examined.

Construction of the composites first involved the definition of a composite grid. The composite grid was chosen to have dimensions equivalent to those of a 40° latitude × 90° longitude domain centered at 35°N, with a fixed number of grid points in the zonal and meridional directions (37 and 17 points, respectively). This definition means that the distance separating the grid points in the zonal direction is a function of the grid row, while the distance separating the grid points in the meridional direction is a constant, equivalent to the distance associated with a 2.5° increment in latitude. Having defined the composite grid, the following procedure was then used to construct the composites for a given cyclone and analysis time:

1) All basic-state variables (such as geopotential height) and derived variables (such as potential vorticity) were placed on the ECMWF latitude–longitude grid.
2) The ECMWF grid point closest to the location of the cyclone's sea level pressure minimum was determined.

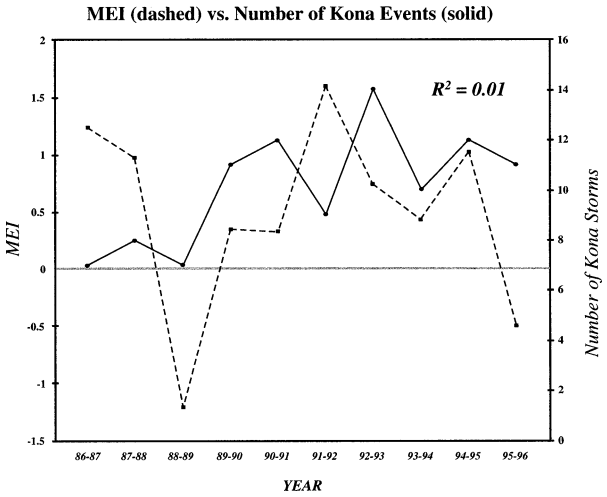

FIG. 7. Number of kona storms in each cool season (solid line) compared to the cool-season average MEI (dashed line); R^2 represents the linear correlation between the two time series.

3) This grid point was taken to represent the center of the composite grid (i.e., the center of the cyclone). The composite grid was then overlaid on the ECMWF latitude–longitude grid such that a given row of the composite grid was superimposed with a given row of the ECMWF grid.
4) A particular grid point on the composite grid was selected. The closest ECMWF grid points to the east and west of this composite grid point were located. The values of each variable at these ECMWF grid points were then linearly interpolated to obtain the value of each variable at the composite grid point. This step was repeated for all composite grid points.

After completing steps 1–4 for all cyclones within a given set of kona storms, the composite distribution of a given variable at each of the three analysis times was then constructed by taking the average of that variable at each of the grid points within the composite grid.

a. CFC cyclones

The structural evolution of the composite CFC cyclone (87 cases) is shown in Fig. 8. At T_{INIT}, the composite CFC cyclone is associated with a narrow, neutrally tilted 300-hPa trough that is flanked by prominent upstream and downstream ridges (Fig. 8a). The 300-hPa trough is firmly embedded within the main belt of the midlatitude westerlies and is located immediately downstream of a relatively weak 300-hPa jet streak. In the lower troposphere (Fig. 8d), a 1010-hPa surface low is embedded within a broad region of high SLP characterized by prominent high pressure centers (>1020 hPa) to the west and northeast of the surface cyclone. At this time, the SLP minimum is located downstream of the 300-hPa trough, which indicates that baroclinic growth of the disturbance is possible. Furthermore, the southwest-to-northeast orientation of the 1000–500-hPa thickness lines near the cyclone center clearly illustrates that CFC cyclones initially develop along a strong baroclinic zone associated with a cold front that has propagated into the subtropical Pacific.

At $T = 0$, the mature CFC cyclone is associated with a much deeper and slightly negatively tilted trough at 300 hPa (Fig. 8b). In the lower troposphere (Fig. 8e), the high pressure center initially located to the west of the surface cyclone at T_{INIT} (Fig. 8d) weakens by this time, while the eastern high pressure center strengthens.

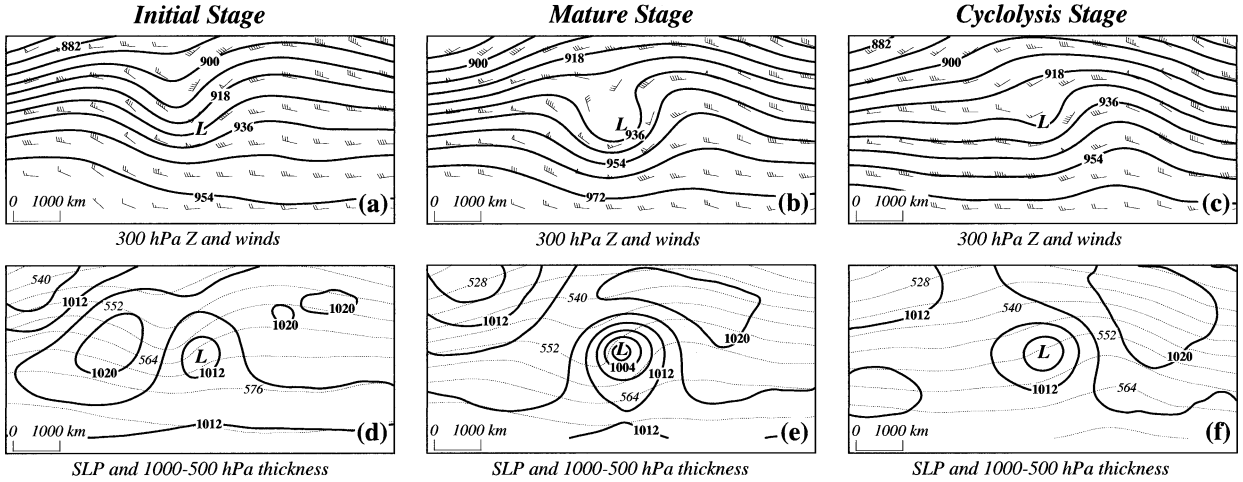

FIG. 8. (a) Composite 300-hPa geopotential height (solid lines) and 300-hPa wind vectors for the T_{INIT} stage of the CFC kona cyclone. Geopotential height labeled in dam and contoured every 9 dam. Wind speeds are indicated by half barb <2.5 m s^{-1}; short barb, 2.5 m s^{-1}; full barb, 5 m s^{-1}; and flag, 25 m s^{-1}. (b) As in (a), except for T_0, the mature stage. (c) As in (a), except for T_{FINL}, the cyclolysis stage. (d) Composite sea level isobars (solid lines) and 1000–500-hPa thicknesses (dashed lines) for the T_{INIT} stage of the CFC kona cyclone. Isobars are labeled in hPa and contoured every 4 hPa. Thickness is labeled in dam and contoured every 6 dam. Position of composite surface low pressure center indicated by the bold "L." (e) As in (d), except for T_0, the mature stage. (f) As in (d), except for T_{FINL}, the cyclolysis stage.

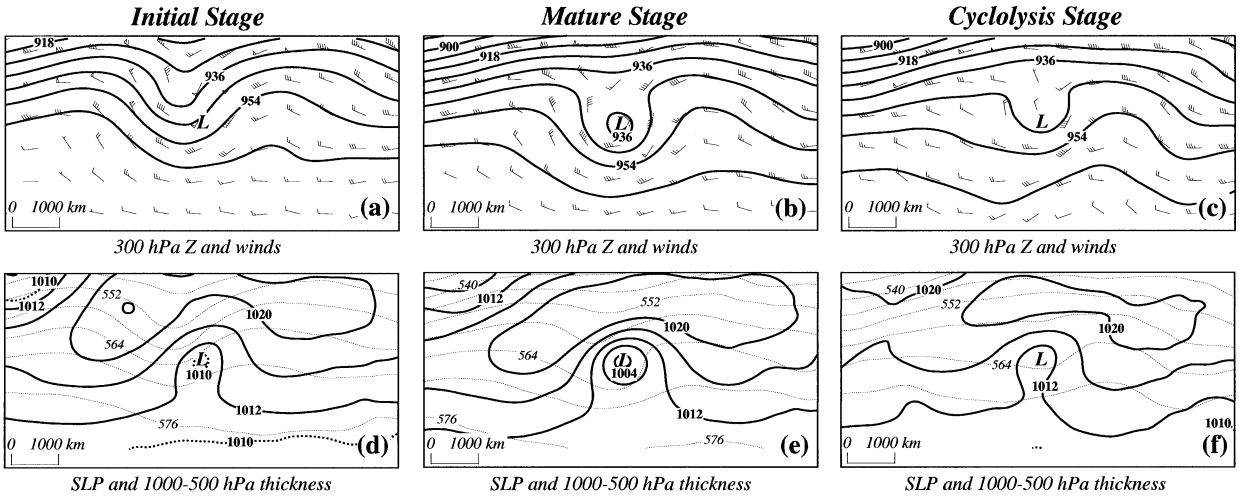

FIG. 9. (a) Composite 300-hPa geopotential height (solid lines) and 300-hPa wind vectors for the T_{INIT} stage (see text for explanation) of the CT kona cyclone. Geopotential height labeled in dam and contoured every 9 dam. Wind speeds are indicated by half barb <2.5 m s^{-1}; short barb, 2.5 m s^{-1}; full barb, 5 m s^{-1}; and flag, 25 m s^{-1}. (b) As in (a), except for T_0, the mature stage. (c) As in (a), except for T_{FINL}, the cyclolysis stage. (d) Composite sea level isobars (solid lines) and 1000–500-hPa thicknesses (short dashed lines) for the T_{INIT} stage for the CT kona cyclone. Isobars are labeled in hPa and contoured every 4 hPa. Long dashed line is the 1010-hPa isobar. Thickness is labeled in dam and contoured every 6 dam. Position of composite surface low pressure center indicated by the bold ''L.'' (e) As in (d), except for T_0, the mature stage. (f) As in (d), except for T_{FINL}, the cyclolysis stage.

Meanwhile, the composite surface cyclone has strengthened to 997 hPa and is now located directly beneath the 300-hPa trough. Note that, by this time, the surface cyclone is located deeper into the cold air (based upon the 1000–500-hPa thicknesses), which likely indicates that the surface cyclone is occluding. Although the 1000–500-hPa thickness field shows that the baroclinic zone has weakened over the center of the surface cyclone, the enhanced thickness gradient northeast of the surface low suggests that a well-defined warm front has developed. In addition, the development of a thickness ridge downstream of the surface cyclone shows that the mature CFC cyclone is characterized by a substantial warm sector. The development of the warm sector is also reflected in the sharper amplitude of the 300-hPa ridge downstream of the surface cyclone (Fig. 8b).

By T_{FINL}, the 300-hPa height and wind fields (Fig. 8c) have undergone an astounding transformation. For instance, the 300-hPa trough associated with the decaying CFC cyclone has weakened considerably, increased its radius of curvature, and moved slightly downstream of the SLP minimum (Fig. 8c). Meanwhile, the 300-hPa ridge upstream of the composite CFC cyclone at $T = 0$ (Fig. 8b) has flattened out so that relatively weak, zonal flow now predominates upstream of the decaying cyclone (Fig. 8c). The weakening of the upper-level features is also reflected at the surface by a weaker composite cyclone (1005 hPa) and the absence of a high pressure center to the west of the surface low (Fig. 8f). Although it is evident that most of the features have weakened by T_{FINL}, it is noteworthy that a well-developed thermal ridge in the 1000–500-hPa thickness field (Fig. 8f) and a robust 300-hPa ridge in the geopotential height field (Fig. 8c) still occur downstream of the composite CFC cyclone.

b. CT cyclones

The structural evolution of the composite CT cyclone (23 cases) is shown in Fig. 9. The incipient CT cyclone is associated with a fairly broad 300-hPa trough that is flanked by broad upstream and downstream ridges (Fig. 9a). Considering the low latitude at which most CT cyclones initially develop (Fig. 3), it is not surprising that the 300-hPa trough is located along the southern edge of a strong geopotential height gradient. The low-latitude development of CT cyclones is also reflected in the location of the surface cyclone along the southern periphery of the subtropical high pressure region, which is characterized by prominent high pressure centers to the northwest and northeast of the surface low (Fig. 9d). The initial development of CT cyclones along a baroclinic zone associated with an advancing cold front is clearly indicated by the strong gradient in the 1000–500-hPa thickness field.

At the mature stage, the composite CT cyclone is characterized by a broad, neutrally tilted trough and weak winds at 300 hPa (Fig. 9b). Examination of the wind field indicates that the mature CT cyclone is located well to the south of the strongest midlatitude westerlies. In the lower troposphere (Fig. 9e), the surface cyclone has strengthened to 1003 hPa and is now located along the southern edge of a moderately strong baroclinic zone. The two surface high pressure centers at T_{INIT} (Fig. 9d) have now merged together to form a continuous band of higher pressure (>1020 hPa) around

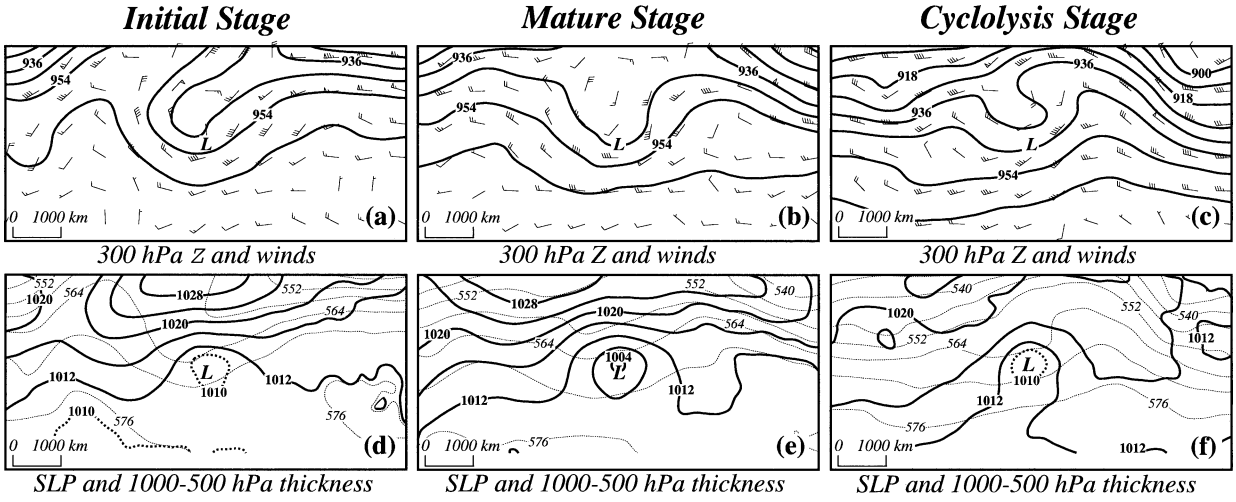

FIG. 10. (a) Composite 300-hPa geopotential height (solid lines) and 300-hPa wind vectors for the T_{INIT} stage (see text for explanation) of the TWE kona cyclone. Geopotential height labeled in dam and contoured every 9 dam. Wind speeds are indicated by half barb <2.5 m s^{-1}; short barb, 2.5 m s^{-1}; full barb, 5 m s^{-1}; and flag, 25 m s^{-1}. (b) As in (a), except for T_0, the mature stage. (c) As in (a), except for T_{FINL}, the cyclolysis stage. (d) Composite sea level isobars (solid lines) and 1000–500-hPa thicknesses (short dashed lines) for the T_{INIT} stage of the TWE kona cyclone. Isobars are labeled in hPa and contoured every 4 hPa. Long dashed line is the 1010-hPa isobar. Thickness is labeled in dam and contoured every 6 dam. Position of composite surface low pressure center indicated by the bold ''L.'' (e) As in (d), except for T_0, the mature stage. (f) As in (d), except for T_{FINL}, the cyclolysis stage.

the northern half of the mature CT cyclone. The strong SLP gradient also indicates that the mature CT cyclone is characterized by strong surface winds along its northern periphery.

By T_{FINL}, the composite CT cyclone has weakened to 1010 hPa and is still located to the south of a broad region of higher pressure (Fig. 9f). At 300 hPa (Fig. 9c), the composite CT cyclone is characterized by a weakened trough and very weak winds. However, the robust downstream ridge has helped to maintain a region of somewhat stronger winds (>40 m s^{-1}) along the southeastern side of the 300-hPa trough. Considering the large number of CT cyclones that decay at far southern latitudes (Fig. 5), the presence of the 300-hPa trough south of the main belt of westerlies (Fig. 9c) and the location of the surface cyclone along the southern boundary of a 1000–500-hPa thickness gradient that weakens throughout the entire evolution (Figs. 9d–f) illustrates that most CT cyclones slowly decay rather than merge with a transient midlatitude trough.

c. TWE cyclones

The structural evolution of the composite TWE cyclone (5 cases) is shown in Fig. 10. Unlike CFC and CT cyclones, the incipient TWE cyclone is associated with a large, positively tilted trough at 300 hPa and a well-developed shear axis that extends northeastward along the axis of the trough (Fig. 10a). At the surface (Fig. 10d), the composite TWE cyclone first appears as a weak trough (1010 hPa) in the SLP field that is located directly south of a strong high pressure center ($\sim$1030 hPa). Similar to CT cyclones, the location of the surface cyclone along the southern periphery of a latitudinal band of higher pressure places the incipient TWE cyclone within a region of large-scale flow characterized by trade wind easterlies in the lower troposphere. Also, the weak 1000–500-hPa thickness gradient (Fig. 10d) indicates that only weak baroclinicity is present during the initial development of TWE cyclones.

At $T = 0$, the composite TWE cyclone is characterized by a very broad, neutrally tilted trough and weak winds at 300 hPa (Fig. 10b). Similar to the mature CT cyclone (Fig. 9b), the strongest 300-hPa winds occur along the southeast side of the 300-hPa trough. In the lower troposphere (Fig. 10e), the composite surface cyclone has strengthened to 1003 hPa and is still located along the southern periphery of a strong high pressure region that spans the entire northern portion of the composite grid.

By T_{FINL}, the 300-hPa trough associated with the composite TWE cyclone has acquired a negative tilt and weakened slightly (Fig. 10c). Although the upstream 300-hPa ridge has also dramatically weakened by this time, a pronounced ridge still occurs downstream of the composite TWE cyclone. The persistence of this downstream ridge has been a notable feature throughout the evolution of each type of kona storm. In the lower troposphere (Fig. 10f), the surface cyclone has weakened to 1009 hPa and is characterized by a well-developed thermal ridge downstream of the surface low.

5. PV perspective of the composite evolution

In their comprehensive review of potential vorticity and its applications to the diagnosis of midlatitude

weather systems, Hoskins et al. (1985) suggested that baroclinic development results from the constructive interaction of a tropopause-level PV anomaly and a near-surface potential temperature (θ) anomaly of like sign. When the tropopause-level PV anomaly is located upshear (i.e., upwind in a thermal wind sense) of the surface θ anomaly, the circulation associated with each can act to lock them into a favorable westward-tilted structure that allows the circulation associated with each anomaly to amplify the other [described as ''mutual reinforcement'' by Davis and Emanuel (1991)]. It was also suggested that the superposition of one anomaly on the other results in an enhanced circulation as the discrete circulations associated with the two anomalies sum to a grander total.

In this portion of the analysis, composite anomalies in the 200–300-hPa-layer averaged PV, 850–700-hPa PV, and 1000-hPa θ were considered for the entire population of kona storms.[4] For each cyclone in the sample, $T = 0$ refers to the mature stage of the cyclone as defined in section 3. In the subsequent analysis, reference will be made to three additional analysis times: $T - 24$ h, $T - 12$ h, and $T + 12$ h, which refer to the moments 24 and 12 h *before,* and 12 h *after,* each cyclone reaches the mature stage. The anomalies for an individual case were calculated using a 6-day time mean, centered at $T = 0$, for that case. This single-case time mean was then subtracted from the instantaneous PV (θ) values for that case at each analysis time to generate single-case anomalies at each time. The 110 single-case anomalies for a given analysis time were then averaged to get the composite anomaly at that time.

In Fig. 11, the positive tropopause-level PV anomalies and the 1000-hPa θ anomalies are shown along with the SLP and 1000-hPa θ for each of the analysis times. At $T - 24$ h (Fig. 11a), the composite surface cyclone was located just downstream of a modest upper PV anomaly. The corresponding PV field (not shown) revealed that this PV feature was still connected to the polar reservoir of higher PV air at this time. Just east of the surface cyclone a well-developed thermal ridge in the 1000-hPa θ field was characterized by an elongated region of positive lower-boundary θ anomalies. By $T - 12$ h (Fig. 11b), the upper PV anomaly had moved closer to the surface cyclone while the 1000-hPa θ anomaly had rotated slightly to the north. Although the amplitude of each anomaly had not changed much from $T - 24$ h, the strengthening of the surface cyclone to 1002 hPa is reflective of the increased superposition of the upper and lower PV anomalies. It is also clear that the upper PV anomaly was positioned at this time so that its associated circulation could subsequently intensify the lower-boundary θ anomaly downstream of the surface cyclone.

By $T = 0$ (Fig. 11c), the upper PV feature (which by this time had become fully separated from the higher PV air to the north) had become more anomalous as it rotated to the southwest of the surface cyclone. Meanwhile, the circulation associated with the upper PV feature had further distorted the 1000-hPa θ field so that both the amplitude and spatial extent of the lower-boundary θ anomaly had greatly increased as it rotated to the northeast of the surface low. The requisite phase tilt for further amplification of the lower θ anomaly was still evident as the upper PV anomaly center remained to the southwest of the lower θ anomaly. Concurrent with the strengthening of each of the PV anomalies, the surface cyclone had also intensified to 998 hPa by this time. Finally, by $T + 12$ h (Fig. 11d), the upper PV feature had weakened slightly and was now collocated with the surface cyclone. Near the surface, a rather robust 1000-hPa θ anomaly had become even more anomalous by this time as it continued to rotate to the northeast of the surface low. The foregoing analysis demonstrates that despite the subtropical origin of kona storms, their development is intimately related to the intrusion of positive tropopause-level PV anomalies of extratropical origin into the subtropics. Furthermore, intensification of the lower-boundary θ anomaly, as a component of the overall development of the composite kona cyclone, clearly supports the notion of kona storms as baroclinic features.

The fact that latent heat release (LHR) operates in the composite kona life cycle is made evident by the prominent downstream ridge that characterizes the 300-hPa flow at the mature stage of each type of kona storm (Figs. 8b, 9b, and 10b). Such ridge building is a certain artifact of LHR. In Fig. 12 an important third component of the PV structure of these storms, the lower-tropospheric PV generated diabatically through LHR, is assessed through consideration of the 850–700-hPa PV anomalies. At $T - 24$ h (Fig. 12a), the lower-tropospheric PV anomaly was located slightly to the northwest of the surface cyclone. A modest superposition of the lower-boundary θ anomaly with the lower-tropospheric PV feature is evident in the composite at this time. By $T - 12$ h (Fig. 12b), the intensities of both the lower-tropospheric PV and 1000-hPa θ anomalies had intensified concurrent with the increased superposition of these two features. Consequently, the composite SLP minimum decreased as well. Further intensification of both anomalies, though slight, occurred during the 12-h period leading to $T = 0$, by which time the cyclone had also become more intense (Fig. 12c). A notable horizontal separation between the lower-tropospheric PV anomaly center and the maximum 1000-hPa θ anomaly existed at $T + 12$ h (Fig. 12d) with the surface cyclone being correspondingly weaker.

The foregoing analysis supports the suggestion that LHR potentially plays a significant role in the life cycle of kona cyclones. In a recent case study of one such storm, Martin and Otkin (2004) employed piecewise PV

[4] Of the 115 kona storms, five cyclones reached the mature stage less than 24 h after the first closed sea level isobar was identified. As a result, these five cyclones were excluded from the composite.

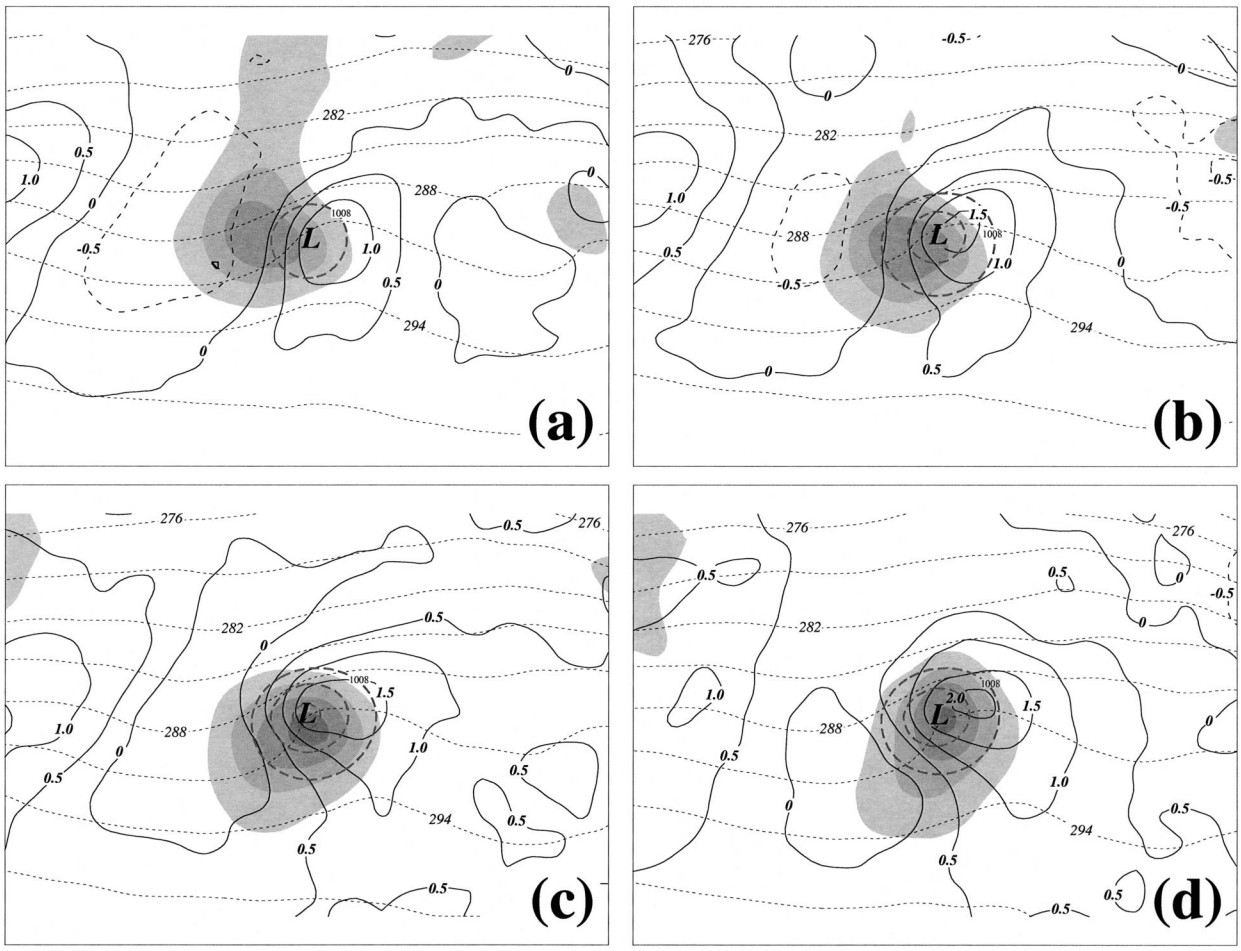

FIG. 11. (a) The 200–300-hPa positive perturbation PV and 1000-hPa potential temperature (θ) perturbations for the composite kona cyclone at $T - 24$ h, with PV perturbations shaded at intervals of 0.5 PVU (1 PVU $= 10^{-6}$ m^2 K kg^{-1} s^{-1}) beginning at 0.25 PVU. Thick solid (dashed) lines are positive (negative) 1000-hPa θ perturbations labeled in K and contoured every 0.5 K. Thin dashed lines are composite 1000-hPa θ labeled in K and contoured every 3 K. Light gray lines are sea level isobars labeled in hPa and contoured every 4 hPa up to 1008 hPa. See text for explanation of how perturbation quantities are calculated. (b) As in (a), but for the composite time $T - 12$ h. (c) As in (a), but for the composite time $T = 0$. (d) As in (a), but for the composite time $T + 12$ h.

inversion to demonstrate that LHR played the *primary* role in both the rapid development and subsequent rapid decay of a cyclone in the central Pacific Ocean. Though that case study and these composite results point toward the establishment of a fundamental role for LHR in subtropical cyclone life cycles, we believe that additional PV-based case studies of kona storms are necessary in order to more broadly characterize the role of diabatically generated PV anomalies in the kona life cycle.

6. Discussion and summary

The kona storm has long been identified as an important feature of the large-scale circulation in the subtropical central and eastern Pacific (SCEP) Ocean. In providing the first climatology of these cyclones, Simpson (1952) documented the frequency of kona storm occurrence and provided a description of certain cyclone characteristics, such as the distribution of wind speeds and precipitation around the surface cyclone. The scope of his study, however, was severely limited by the lack of data across the Pacific Ocean basin. Taking advantage of the availability of modern gridded datasets, the present study has employed 10 yr of data from the ECMWF TOGA dataset to provide an updated synoptic climatology of the subtropical kona storm and to extend our knowledge of the frequency of kona storm occurrence.

The updated climatology was constructed by manually tracking all surface cyclones (identified as minima in the SLP field surrounded by at least one closed isobar) across the North Pacific basin. As a basic requirement to qualify as a kona storm, a surface cyclone had to initially develop within a portion of the subtropical Pacific. According to the several constraints outlined in section 3, 115 kona storms were identified in the SCEP (10°–40°N, 160°E–130°W) during the 10-yr period. Three distinct types of kona storms were identified:

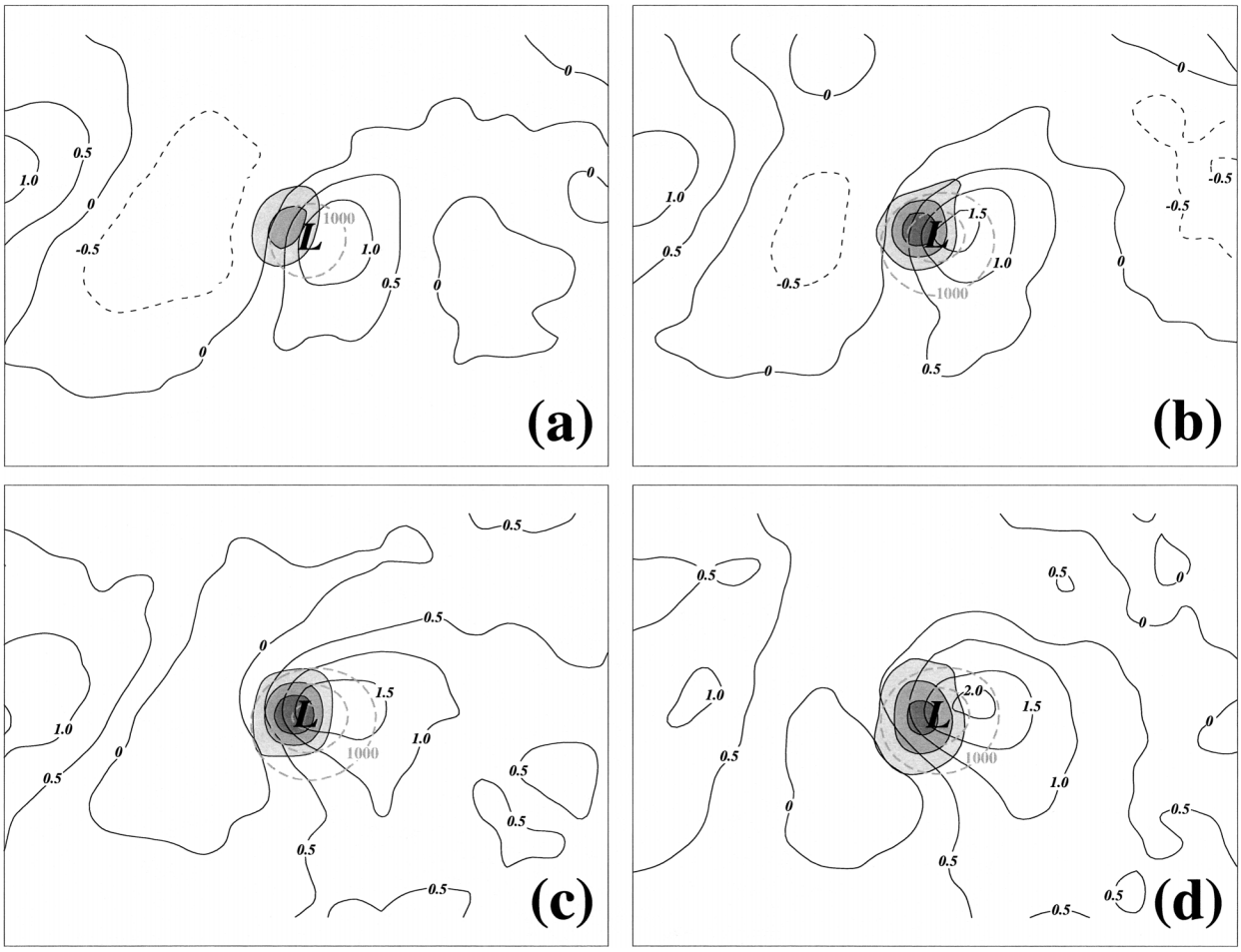

FIG. 12. The 850–700-hPa positive potential vorticity anomaly (PV') and 1000-hPa potential temperature (θ) perturbations for the composite kona cyclone at $T - 24$ h, with PV' shaded at intervals of 0.05 PVU (1 PVU $= 10^{-6}$ m^2 K kg^{-1} s^{-1}) beginning at 0.05 PVU. The 1000-hPa θ perturbations are labeled and contoured as in Fig. 11. Light gray lines are sea level isobars labeled in hPa and contoured every 1 hPa up to 1000 hPa. (b) As in (a), but for the composite time $T - 12$ h. (c) As in (a), but for the composite time $T = 0$. (d) As in (a), but for the composite time $T + 12$ h.

cold-frontal cyclogenesis (CFC) cyclones, trade wind easterlies (TWE) cyclones, and cold-frontal cyclogenesis/trade wind easterlies (CT) cyclones, the former two previously identified by Simpson (1952). Of the three types, it was found that CFC cyclones are the most common type of kona storm (87 cases) while CT and TWE cyclones occur much less frequently (23 and 5 cases, respectively).

The geographical distribution of kona storms at the initial development, mature, and final cyclolysis stages of cyclone evolution was examined. From this examination, it was found that kona storms exhibit substantial interannual variability in the distribution of initial cyclone locations. A distinct latitudinal stratification was also evident for each type of kona storm with CFC, CT, and TWE cyclones each more likely to initially develop at successively lower latitudes. At the mature stage, most kona storms were concentrated along the northern portion of the SCEP domain with only a few CT and TWE cyclones still located south of 25°N. The relatively uniform distribution of kona storms across the eastern half of the Pacific basin during the decay stage indicates that kona cyclolysis does not occur within a favored geographical region for the population as a whole; CT cyclones, however, did show a preference to decay within a small region west of Hawaii. Construction of a ''propagation rose'' demonstrated that kona storms can propagate in any direction but exhibit a preference to propagate toward the northeast.

The cumulative monthly distribution of kona storms revealed that these cyclones preferentially occur during late autumn (October–November), with a notable decrease in cyclone frequency during the midwinter months (December–January). This result differs from the climatology presented by Simpson (1952) in which a maximum in kona activity was reported for January. That study employed both a smaller analysis domain and a less comprehensive dataset than the present in-

vestigation, likely contributing to an underestimate of the frequency of fall and spring cyclones in the SCEP. The apparent seasonal cycle in cyclone frequency revealed by the present study suggests that changes in the large-scale circulation, most notably the strength and zonal extent of the Asian jet, could modulate the occurrence of kona storms. The reduction of kona cyclone frequency during the midwinter months reported in this study is consistent with the fact that the Asian jet is climatologically strongest during midwinter. Further support for a connection between kona frequency and characteristics of the Asian jet was offered by Chu et al. (1993). In an analysis of the large-scale circulation associated with two winter seasons (January–February), they showed that the season characterized by numerous (zero) ''kona days'' was also associated with a weakened (strengthened) Asian jet. This connection is robustly confirmed by the companion examination of the large-scale circulations associated with periods of enhanced or diminished subtropical cyclone activity in the SCEP undertaken by Otkin and Martin (2004, hereafter OM).

Considerable interannual variability in the number of kona storms that developed in the SCEP was also noted. Although previously documented changes in the large-scale circulation and basinwide upper-tropospheric PV structure (Shapiro et al. 2001) associated with opposite phases of ENSO were considered to potentially underlie this variability, calculations using the multivariate ENSO index uncovered no correlation between the phase of ENSO and the annual number of kona storms.

In an attempt to better understand the synoptic setting within which each type of kona storm evolved, the composite structure and evolution of the 87 CFC, 23 CT, 5 TWE cyclones observed during the 10-yr climatology was considered. A separate analysis of the composite evolution of 110 kona storms from a PV perspective was also undertaken. These analyses revealed certain characteristics that were common to all kona storms. Among these common characteristics were the following:

1) The initial development of each of the three composite cyclones was associated with a preexisting trough in the 300-hPa geopotential height field. The PV analysis for all kona storms showed that this trough was characterized by a modest upper PV anomaly. The corresponding PV field revealed that this PV anomaly was attached to the polar reservoir of higher PV air until the mature phase. This indicates that kona cyclone development, regardless of type, results from the intrusion of an upper-tropospheric disturbance of extratropical origin into the subtropics.
2) As indicated by the 1000–500-hPa thickness field, the evolution of all kona storms in the climatology occurred along a preexisting baroclinic zone in the lower troposphere. The strength of this baroclinic zone varied for each type of kona storm, with CFC (TWE) cyclones characterized by the strongest (weakest) baroclinic zone. Also, the predominance of a westward-tilted geopotential height structure in each of the composites at the initial time indicates that kona storms undergo a period of baroclinic growth during the early stages of their life cycle.
3) Weak 300-hPa winds were present throughout the evolution of each type of kona storm. This was especially evident for the composite CT and TWE cyclones. The presence of weak winds in each of the composites is consistent with the results of OM, who found that active periods of subtropical cyclogenesis in the SCEP were characterized by anomalously weak winds at 300 hPa.
4) The mature surface cyclone associated with each type of kona storm was nestled to the south of a broad region of higher SLP.
5) Each type of kona storm was characterized by the development of a robust ridge in the 300-hPa geopotential height field downstream of the composite cyclone. The development of this ridge was reflected in the lower troposphere by a pronounced thermal ridge in the 1000–500-hPa thickness field. From a PV perspective, this thermal ridge was associated with a large region of positive lower-boundary θ anomalies and may also be evidence of a diabatic contribution to the kona life cycle.

While all kona storms exhibited the above characteristics, important differences in the evolution of the 300-hPa trough were also noted for each type of kona storm. For instance, although the initial development of each composite cyclone was associated with a preexisting 300-hPa trough, the structure and location of this trough relative to the strongest midlatitude westerlies varied greatly for each type of kona storm. For example, the composite CFC and CT cyclones were characterized by a relatively narrow, neutrally tilted trough while the composite TWE cyclone was associated with a much broader, strongly positively tilted trough. At this time, the trough associated with the composite CFC cyclone was firmly embedded within the strongest midlatitude westerlies while the troughs associated with the composite CT and TWE cyclones were located along the equatorward edge, and well to the south, of the strongest westerlies, respectively. By the mature stage, the trough associated with the composite CFC cyclone was still embedded within the strongest westerlies while the composite CT and TWE cyclones had become fully separated from the strongest westerlies. Finally, it was shown that the mature CT cyclone tends to slowly decay rather than merge with a transient midlatitude trough, as was the case for the composite CFC and TWE cyclones.

Finally, the climatology reveals substantial intraseasonal variability in the frequency of kona storms, with certain periods characterized by the development of numerous kona storms while other periods were complete-

ly void of kona storms. The presence of such variability renders it tempting to suggest that intraseasonal fluctuations in the large-scale circulation across the Pacific basin may modulate the occurrence of kona storms. Support for this notion is provided by Chu et al. (1993). They showed that numerous (zero) ''kona days'' occurred during the winter season characterized by the negative (positive) phase of the Pacific–North America (PNA) pattern (Wallace and Gutzler 1981) and by a weakened (strengthened) and zonally retracted (elongated) Asian jet. Although this study only covered two winter seasons, it provides tantalizing evidence that changes in the large-scale circulation can modulate the temporal distribution of kona storms. In order to address these issues, the companion paper (OM) will explore the influence of the Asian jet and the PNA pattern in modulating the occurrence of kona storms in the SCEP. In addition, Rossby wave dispersion away from anomalous tropical convection in the central Pacific as well as barotropic energy conversions will be evaluated as possible mechanisms for forcing an extratropical response that is conducive to the development of kona storms.

Acknowledgments. The authors wish to thank the European Centre for Medium Range Weather Forecasts for providing the data used in this study. The constructive comments of two anonymous reviewers greatly enhanced the presentation of the manuscript. This work was sponsored by the National Science Foundation under Grant ATM-0202012.

REFERENCES

Businger, S., T. Birchard, K. Kodama, P. Jendrowski, and J.-J. Wang, 1998: A bow echo and severe weather associated with a Kona low in Hawaii. *Wea. Forecasting,* **13,** 576–591.

Chu, P.-S., A. J. Nash, and F.-Y. Porter, 1993: Notes and correspondence: Diagnostic studies of two contrasting rainfall episodes in Hawaii: Dry 1981 and wet 1982. *J. Climate,* **6,** 1457–1462.

Cram, R. S., and H. R. Tatum, 1979: Record torrential rainstorms on the island of Hawaii, January–February 1979. *Mon. Wea. Rev.,* **107,** 1653–1662.

Dangerfield, L. H., 1921: Kona storms. *Mon. Wea. Rev.,* **49,** 327–328.

Davis, C. A., and K. A. Emanuel, 1991: Potential vorticity diagnostics of cyclogenesis. *Mon. Wea. Rev.,* **119,** 1929–1953.

Geisler, J. E., M. L. Blackmon, G. T. Bates, and S. Munoz, 1985: Sensitivity of January climate response to the magnitude and position of equatorial Pacific sea surface temperature anomalies. *J. Atmos. Sci.,* **42,** 1037–1049.

Hoerling, M. P., A. Kumar, and M. Zhong, 1997: El Niño, La Niña, and the nonlinearity of their teleconnections. *J. Climate,* **10,** 1769–1786.

Horel, J. D., and J. M. Wallace, 1981: Planetary-scale atmospheric phenomena associated with the Southern Oscillation. *Mon. Wea. Rev.,* **109,** 813–829.

Hoskins, B. J., M. E. McIntyre, and A. W. Robertson, 1985: On the use and significance of isentropic potential vorticity maps. *Quart. J. Roy. Meteor. Soc.,* **111,** 877–946.

Kidson, J. W., M. J. Revell, B. Bhaskaran, A. B. Mullan, and J. A. Renwick, 2002: Convection patterns in the tropical Pacific and their influence on the atmospheric circulation at higher latitudes. *J. Climate,* **15,** 137–159.

Kodama, K., and G. M. Barnes, 1997: Heavy rain events over the south-facing slopes of Hawaii: Attendant conditions. *Wea. Forecasting,* **12,** 347–367.

Lau, K.-M., and T. J. Phillips, 1986: Coherent fluctuations of extratropical geopotential height and tropical convection in intraseasonal time scales. *J. Atmos. Sci.,* **43,** 1164–1181.

Leopold, L. B., 1948: Diurnal weather patterns on Oahu and Lanai, Territory of Hawaii. *Pac. Sci.,* **2,** 81–95.

Lyons, S. W., 1982: Empirical orthogonal function analysis of Hawaiian rainfall. *J. Appl. Meteor.,* **21,** 1713–1729.

Martin, J. E., and J. A. Otkin, 2004: The rapid growth and decay of an extratropical cyclone over the central Pacific Ocean. *Wea. Forecasting,* **19,** 358–376.

Morrison, I., and S. Businger, 2001: Synoptic structure and evolution of a Kona low. *Wea. Forecasting,* **16,** 81–98.

Otkin, J. A., and J. E. Martin, 2004: The large-scale modulation of subtropical cyclogenesis in the central and eastern Pacific Ocean. *Mon. Wea. Rev.,* in press.

Ramage, C. S., 1962: The subtropical cyclone. *J. Geophys. Res.,* **67,** 1401–1411.

Riehl, H., 1949: Some aspects of Hawaiian rainfall. *Bull. Amer. Meteor. Soc.,* **30,** 176–187.

Schroeder, T. A., 1977a: Meteorological analysis of an Oahu flood. *Mon. Wea. Rev.,* **105,** 458–468.

——, 1977b: Hawaiian waterspouts and tornadoes. *Mon. Wea. Rev.,* **105,** 1163–1170.

Shapiro, M. A., H. Wernli, N. A. Bond, and R. Langland, 2001: The influence of the 1997–99 El Niño Southern Oscillation on extratropical baroclinic life cycles over the eastern North Pacific. *Quart. J. Roy. Meteor. Soc.,* **127,** 331–342.

Simpson, R. H., 1952: Evolution of the kona storm, a subtropical cyclone. *J. Meteor.,* **9,** 24–35.

Wallace, J. M., and D. M. Gutzler, 1981: Teleconnections in the geopotential height field during the Northern Hemisphere winter. *Mon. Wea. Rev.,* **109,** 784–812.

Wang, H., and R. Fu, 2000: Winter monthly mean atmospheric anomalies over the North Pacific and North America associated with El Niño SSTs. *J. Climate,* **13,** 3435–3447.

Wang, J.-J., H.-M. Juang, K. Kodama, S. Businger, Y.-L. Chen, and J. Partain, 1998: Application of the NCEP Regional Spectral Model to improve mesoscale weather forecasts in Hawaii. *Wea. Forecasting,* **13,** 560–575.

Wolter, K., and M. S. Timlin, 1993: Monitoring ENSO and COADDS with a seasonally adjusted principal component index. *Proc. 17th Climate Diagnostics Workshop,* Norman, OK, NOAA/NMC/CAC, 52–57.